arXiv:1212.0221v1 [cond-mat.str-el] 2 Dec 2012

Interplay between $3d$- and $4f$-electrons in Co-doped CeFeAsO

T. Shang,[1] L. Yang,[1] Y. Chen,[1] J. L. Zhang,[1] L. Jiao,[1] J. Chen,[1] J. Dai,[2] and H. Q. Yuan[1,*]

[1] *Department of Physics and Center for Correlated Matter, Zhejiang University, Hangzhou, 310027, China*
[2] *Condensed Matter Group, Department of physics,*
Hangzhou Normal University, Hangzhou 310036, China

(Dated: December 4, 2012)

We report the tunable interplay between $3d$- and $4f$-electrons and the relevant physical properties in polycrystalline $\mathrm{CeFe}_{1-x}\mathrm{Co}_x\mathrm{AsO}$ ($0 \leq x \leq 1$) by means of measuring the electrical resistivity $\rho(T)$, magnetic susceptibility $\chi(T)$ and specific heat $C(T)$. CeFeAsO undergoes a spin-density-wave (SDW) transition associated with Fe $3d$-electrons around 150 K, which is rapidly suppressed by Fe/Co substitution. Superconductivity appears in a narrow doping range of $0.05 < x < 0.2$, showing a maximum transition temperature of $T_{\mathrm{sc}} \approx 13.5$ K around $x = 0.1$. On the other hand, Ce $4f$-electrons form an antiferromagnetic (AFM) state over the entire doping range; the Néel temperature $T_{\mathrm{N}}^{\mathrm{Ce}}$ increases upon suppressing the SDW transition of Fe and then remains nearly unchanged with further increasing Co concentration up to $x \simeq 0.8$ ($T_{\mathrm{N}}^{\mathrm{Ce}} \approx 4$K). On the Co-rich side ($x \geq 0.75$), Co $3d$-electrons are ferromagnetically ordered; its Curie temperature reaches $T_{\mathrm{C}}^{\mathrm{Co}} \approx 75$ K at $x = 1$. Furthermore, evidence of Co-induced polarization on Ce-moments is observed in this regime. Our results suggest that the effects of both electron hybridizations and magnetic exchange coupling between the $3d$-$4f$ electrons give rise to a rich phase diagram in the alloy $\mathrm{CeFe}_{1-x}\mathrm{Co}_x\mathrm{AsO}$.

PACS number(s): 74.70.Xa,71.20.Eh,75.20.Hr

I. INTRODUCTION

The discovery of superconductivity in $\mathrm{LaFeAsO}_{1-x}\mathrm{F}_x$ has stimulated intensive efforts on searching for new materials with higher superconducting transition temperature T_{sc} and revealing their unconventional nature.[1] Among the iron-based superconductors (FeSCs), the 1111-type compounds *Re*Fe*Pn*O (*Re* = rare earth, *Pn* = pnictogen) demonstrate fantastic properties, showing the highest T_{sc} among the FeSCs.[2] Furthermore, the rare earth elements usually form an antiferromagnetically ordered state at very low temperatures. For instance, CeFeAsO subsequently undergoes two AFM-type transitions upon cooling down from room temperature, one associated with Fe ($T_{\mathrm{N}}^{\mathrm{Fe}} \approx 150$ K) and the other one attributed to Ce ($T_{\mathrm{N}}^{\mathrm{Ce}} \approx 3.4$ K).[3,4] On the other hand, CeFePO is a paramagnetic (PM) heavy fermion metal.[5] Recent studies demonstrated that a ferromagnetic (FM) state of Ce $4f$-electrons, separating the AFM state from the PM heavy fermion state, develops in the intermediate doping region in $\mathrm{CeFeAs}_{1-x}\mathrm{P}_x\mathrm{O}$.[6–8] These indicate that the 1111-type iron pnictides may provide us a rare system to study the interplay of $4f$- and $3d$-electrons, and their emergent properties. A systematic study of the interplay between $4f$- and $3d$-electrons would help elucidate the nature of superconductivity and magnetism in iron pnictides.

In *Re*FeAsO, Fe/Co substitution presents an alternative example, in which extra electrons are introduced into the FeAs layers. Upon substituting Fe with Co, the magnetic/structural transition of Fe is quickly suppressed and superconductivity exists over a narrow doping range.[9–13] On the other hand, the Co-end compounds, namely *Re*Co*Pn*O, demonstrate rich magnetic properties. For example, CeCoAsO and CeCoPO exhibit an enhanced Sommerfeld coefficient ($\sim$200 mJ/mol-K^2), and their Co-ions undergo a FM transition at $T_{\mathrm{C}}^{\mathrm{Co}} = 75$ K.[14,15] In the $\mathrm{GdFe}_{1-x}\mathrm{Co}_x\mathrm{AsO}$ case, we found that Co $3d$-electrons undergo a ferromagnetic transition at $x > 0.8$, which transition temperature increases with increasing Co content, reaching $T_{\mathrm{C}}^{\mathrm{Co}} = 75$ K in GdCoAsO.[16] At lower temperatures, the large moment of Gd is robust against the FM order of Co, and maintains its AFM order with a nearly unchanged Néel temperature over the entire doping concentration. However, the coupling between the Gd and Co sublattices leads to ferrimagnetic behavior and also a possible magnetic reorientation. In contrast to Gd, the $4f$-electrons in $\mathrm{CeFe}_{1-x}\mathrm{Co}_x\mathrm{AsO}$ carry a smaller magnetic moment. As a result, the interplay between $4f$- and $3d$-electrons may cause different behavior in $\mathrm{CeFe}_{1-x}\mathrm{Co}_x\mathrm{AsO}$. In a previous work,[9] it was mainly devoted to the studies of magnetism and superconductivity on the Fe-rich side, a systematic study of the emergent behavior in $\mathrm{CeFe}_{1-x}\mathrm{Co}_x\mathrm{AsO}$ is, therefore, highly desirable.

In this paper, we study the phase diagram of $\mathrm{CeFe}_{1-x}\mathrm{Co}_x\mathrm{AsO}$ ($0 \leq x \leq 1$) by measuring the transport, magnetic and thermodynamic properties. We confirmed that the magnetic/structural transition of Fe is quickly suppressed by Fe/Co substitution and superconductivity appears in a narrow doping range ($0.05 < x < 0.2$), with a maximum $T_{\mathrm{sc}} \approx 13.5$ K around $x = 0.1$. On the other hand, Ce-ions undergo an AFM transition at low temperatures in the entire doping range. Its Néel temperature, $T_{\mathrm{N}}^{\mathrm{Ce}}$, increases upon suppressing the SDW transition of Fe, and then remains nearly unchanged with further increasing Co content, indicating a possible competing interaction between Ce $4f$- and Fe $3d$- electrons on the Fe-side. For $x \geq 0.75$, Co-$3d$ electrons become ferromagnetically ordered and its Curie temperature $T_{\mathrm{C}}^{\mathrm{Co}}$ increases with increasing x, causing a strong polarization

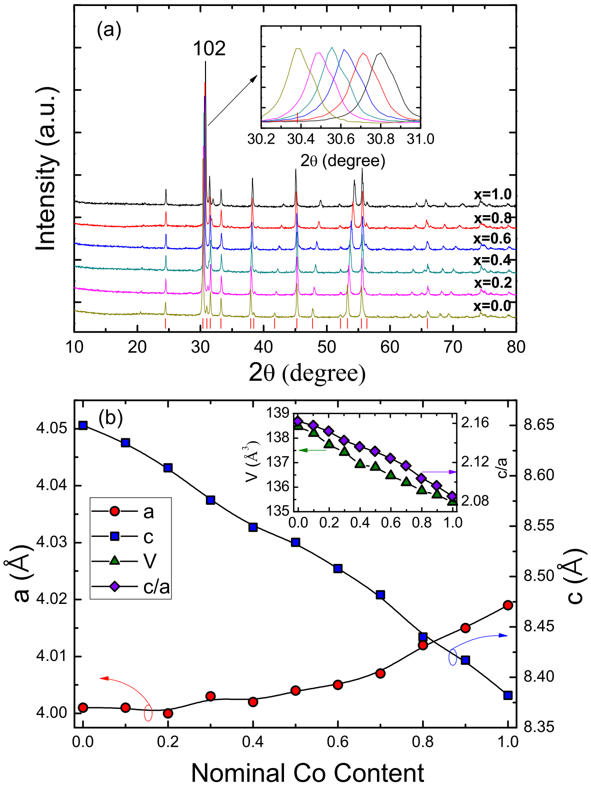

FIG. 1. (Color online) Powder X-ray diffraction patterns and the lattice parameters of $\mathrm{CeFe}_{1-x}\mathrm{Co}_x\mathrm{AsO}$. (a) Room temperature XRD patterns for the samples with $x = 0.0, 0.2, 0.4, 0.6, 0.8, 1.0$. The inset shows the enlarged (**102**) peaks. (b) Lattice parameters as a function of nominal Co content. The inset plots the unit cell volume (left axis) and the c/a ratio (right axis) as a function of doping.

effect on Ce-moments. Our findings indicate that the Fe/Co substitution may effectively tune the interplay of $3d$-$4f$ electrons in $\mathrm{CeFe}_{1-x}\mathrm{Co}_x\mathrm{AsO}$, leading to rich physical properties.

II. EXPERIMENTAL DETAILS

Polycrystalline samples of $\mathrm{CeFe}_{1-x}\mathrm{Co}_x\mathrm{AsO}$ ($0 \leq x \leq 1$) were synthesized in evacuated quartz ampoules by a two-step solid state reaction method. High-purity Ce (99.8%) and As (99.999%) chunks, also $\mathrm{Co}_3\mathrm{O}_4$ (99.97%), $\mathrm{Fe}_2\mathrm{O}_3$ (99.99%), Fe(99.9%) and Co(99.9%) powders were used as raw materials. The dehydrated $\mathrm{Co}_3\mathrm{O}_4$ and $\mathrm{Fe}_2\mathrm{O}_3$ were prepared by heating the powders at 1173 K for 10 h in atmosphere. First, Ce and As chunks were mixed and the pure phase CeAs was prepared by heating the mixture in a sealed evacuated quartz ampoule at 1073 K for 24 h, and then at 1323 K for 48 h. Then, CeAs, $\mathrm{Co}_3\mathrm{O}_4$, $\mathrm{Fe}_2\mathrm{O}_3$, Fe and Co powders were weighed according to the stoichiometric ratio, thoroughly ground, and pressed into pellets. The entire process was carried out in an argon-filled glove box. Finally, the pellets were sealed into evacuated quartz ampoules, then slowly heated to 1323 K at a rate of 100 K/h and kept at this temperature for one week to obtain sintered pellets.

The structure of the polycrystalline samples was characterized by powder X-ray diffraction (XRD) at room temperature using a PANalytical X'Pert MRD diffractometer with Cu Kα radiation and a graphite monochromator. Measurements of the DC magnetic susceptibility and specific heat were carried out in a Quantum Design Magnetic Property Measurement System (MPMS-5T) and Physical Property Measurement System (PPMS-9T), respectively. Temperature dependence of the electrical resistivity was measured by a standard four-point method from 3K to 300 K in a closed cycle refrigerator.

III. RESULTS AND DISCUSSION

A. Crystal Structure

Figure 1(a) plots six representative XRD patterns of the $\mathrm{CeFe}_{1-x}\mathrm{Co}_x\mathrm{AsO}$ samples ($0 \leq x \leq 1$). The vertical bars on the bottom denote the theoretically calculated positions of the Bragg diffractions for CeFeAsO. All the peaks can be well indexed based on the tetragonal ZrCuSiAs structure with a space group of P4/nmm. No obvious impurity phases are detected, indicating a high quality of these samples. The shift of the (**102**) peak toward the right (larger 2θ value) with increasing x, as shown in the right inset of Fig.1(a), reveals a contraction of the crystal lattice with increasing Co-concentration. The lattice parameters, refined by the least square fitting, are plotted as a function of nominal Co-concentration in Fig.1(b). Different from $\mathrm{CeFeAs}_{1-x}\mathrm{P}_x\mathrm{O}$ where both the a- and c-axis shrink with increasing P-content,[6] in $\mathrm{CeFe}_{1-x}\mathrm{Co}_x\mathrm{AsO}$ the c-axis shrinks significantly while the a-axis increases slightly with increasing Co concentration, meaning that Fe/Co substitution increases three dimensionality in comparison with As/P substitution. This becomes more pronounced above $x \approx 0.75$, for which Co-electrons are ferromagnetically ordered at low temperatures. The shrinkage of the c-axis reduces the distance between the CeO and Fe(Co)As layers, and thus enhances the hybridizations between $3d$- and $4f$-electrons. The inset of Fig.1(b) shows the unit cell volume and the c/a ratio versus Co concentration, both of which monotonically decrease with increasing x. The former decreases by 2.22% at $x = 1$. The shift of the XRD patterns and the variation of lattice parameters suggest that the Co atoms are successfully incorporated into the crystal lattice.

B. Electrical Resistivity

Temperature dependence of the normalized electrical resistivity is shown in Fig.2 for $\mathrm{CeFe}_{1-x}\mathrm{Co}_x\mathrm{AsO}$ ($0 \leq x \leq 1$). The resistive anomaly observed around $T_{\mathrm{SDW}} \approx$

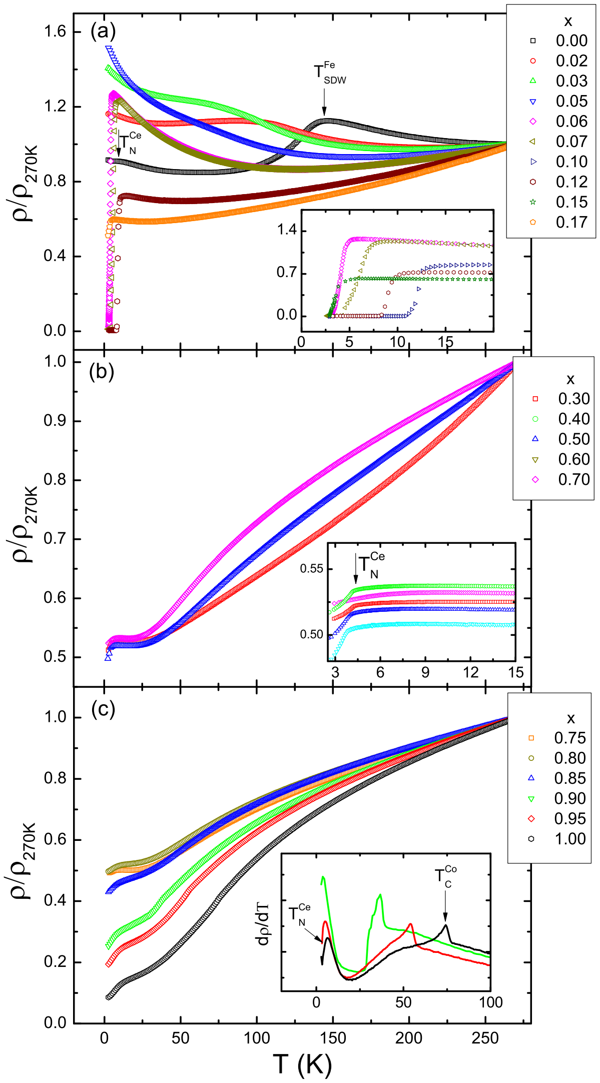

FIG. 2. (Color online) Temperature dependence of the normalized electrical resistivity of $\mathrm{CeFe}_{1-x}\mathrm{Co}_x\mathrm{AsO}$. (a) $0 \leq x \leq 0.2$. (b) $0.3 \leq x \leq 0.7$. (c) $0.75 \leq x \leq 1$. The insets of (a) and (b) expand the low temperature regime. The inset of (c) shows the derivative plots of the electrical resistivity with respect to temperature for $x = 0.9$, 0.95 and 1, from which the transition temperatures of T_N^{Ce} and T_C^{Co} can be determined.

TABLE I. The superconducting transition temperatures T_{sc} (K) for $0.07 \leq x \leq 0.2$, determined from the 90% (T_{sc}^{ρ} (onset)), 50% (T_{sc}^{ρ} (mid)) and 10% (T_{sc}^{ρ} (zero)) of the normal resistivity at T_{sc} and the onset of magnetic susceptibility T_{sc}^{χ}.

x	T_{sc}^{ρ} (onset)	T_{sc}^{ρ} (mid)	T_{sc}^{ρ} (zero)	T_{sc}^{χ}
0.06	4.7	3.95	3.2	4.6
0.07	7.8	6.1	4.4	5
0.10	13.5	11.7	11.1	13
0.12	11	9.7	8.4	9.1
0.15	5.9	4.4	2.9	No
0.17	4.5	No	No	No

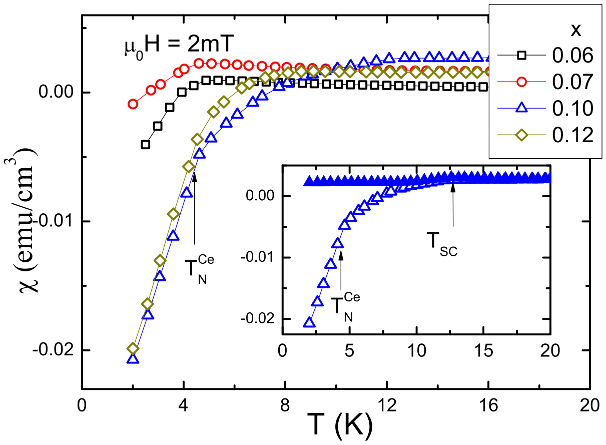

FIG. 3. (Color online) Low temperature magnetic susceptibility $\chi(T)$ for $\mathrm{CeFe}_{1-x}\mathrm{Co}_x\mathrm{AsO}$, $0.06 \leq x \leq 0.12$. The open and filled symbols show the data measured at zero-field cooling (ZFC) and field cooling (FC), respectively. To demonstrate the existence of an AFM transition of Ce below T_{sc}, we plot $\chi(T)$ for $x = 0.1$ in the inset, from which a kink at T_N^{Ce} can be identified.

150 K in CeFeAsO characterizes the almost degenerate SDW-transition of Fe $3d$-electrons and the tetragonal to orthorhombic structural phase transition.[3,4,17] With further decreasing temperature, another resistive kink appears around $T_N^{\mathrm{Ce}} \approx 4$ K, marking the AFM transition of Ce.[3,4] Upon partially substituting Fe with Co, the transition at T_{SDW} is quickly suppressed and becomes hardly visible above $x \approx 0.06$. Meanwhile, superconductivity appears around $x = 0.06$, and the transition temperature reaches a maximum of $T_{\mathrm{sc}}^{\mathrm{onset}} \approx 13.5$ K at $x = 0.1$ (see the inset of Fig.2(a)). Note that, for $0.06 \leq x \leq 0.17$, no signature of magnetic transition can be identified below T_{sc} in the electrical resistivity, being different from that of $\mathrm{CeFeAsO}_{1-x}\mathrm{F}_x$ in which a non-zero resistive transition shows up below T_{sc} attributed to the magnetic order of Ce.[18] However, evidence for the AFM transition of Ce can be inferred from the magnetic susceptibility and specific heat (see below). In comparison with $\mathrm{CeFeAsO}_{1-x}\mathrm{F}_x$,[3] another difference is the low-temperature semiconducting behavior observed in the underdoped $\mathrm{CeFe}_{1-x}\mathrm{Co}_x\mathrm{AsO}$ ($x < 0.1$), which may originate from the disorder effect or the Kondo-like scattering. The tiny amount of Co atoms in the materials may act as magnetic impurities, leading to a resistive minimum as a result of Kondo effect. The system eventually becomes metallic with further increasing Co concentration. Figure 2(b) presents the normalized electrical resistivity for $0.3 \leq x \leq 0.7$, which decreases monotonically with decreasing temperature. In this doping region, only one pronounced resistive transition is seen around 4 K, which is attributed to the AFM transition of Ce $4f$-electrons, as shown by the arrow in the inset of Fig.2(b). For $x \geq 0.75$, the electrical resistivity demonstrates stronger temperature dependence

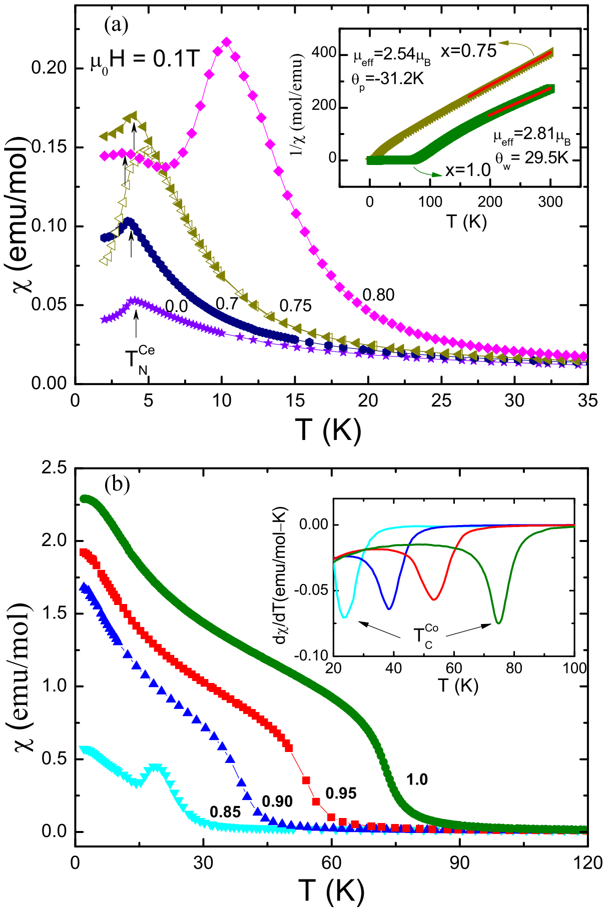

FIG. 4. (Color online) Temperature dependence of the DC magnetic susceptibility for $\mathrm{CeFe}_{1-x}\mathrm{Co}_x\mathrm{AsO}$, $0 \le x \le 1$. The open and filled symbols present the ZFC and FC data, respectively. The upper inset plots the inverse susceptibility as a function of temperature for $x = 0.75$ and $x = 1$. The red lines are fits to Curie-Weiss law. The Curie temperature $T_{\mathrm{C}}^{\mathrm{Co}}$ of Co is determined from the negative peak position of the derivative $\mathrm{d}\chi(T)/\mathrm{d}T$ as shown in the lower inset.

with a broad hump around 100 K, likely attributed to the enhanced $3d$-$4f$ hybridizations as typically found in some Kondo lattice compounds.[19,20] Upon further cooling down, the system undergoes two subsequent transitions as clearly shown in the derivatives of the electrical resistivity with respective to temperature, $d\rho/dT$, in the inset of Fig.2(c), one corresponding to the FM transition of Co ($T_{\mathrm{C}}^{\mathrm{Co}}$) and the other one for the AFM order of Ce ($T_{\mathrm{N}}^{\mathrm{Ce}}$), both shifting to higher temperature with further increasing Co concentration. The magnetic transition of Ce is broadened on the Co-rich side; we attribute it to the polarization effect of Co-ferromagnetism which will be further illustrated in terms of magnetic susceptibility and specific heat.

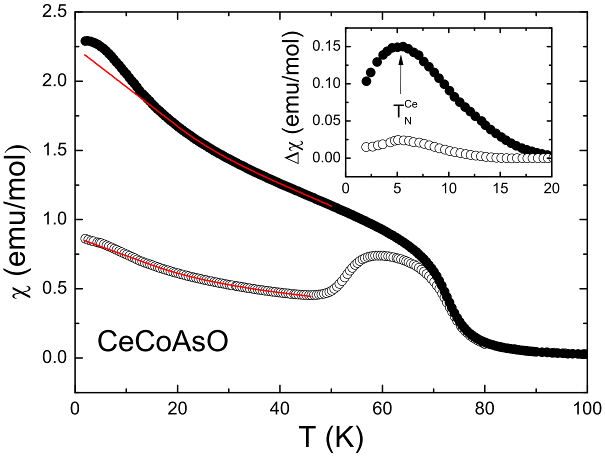

FIG. 5. (Color online) Temperature dependence of the magnetic susceptibility $\chi(T)$ for CeCoAsO. The open and filled circles show the ZFC and FC data, respectively. The red lines present a polynomial fit to the experimental data in the temperature range of 20 K to 40 K, which are treated as the FM background of Co. The inset plots the magnetic susceptibility after subtracting the FM background.

C. Magnetic Properties

DC magnetization of $\mathrm{CeFe}_{1-x}\mathrm{Co}_x\mathrm{AsO}$ was measured as functions of temperature and magnetic field. Figure 3 shows the magnetic susceptibility $\chi(T)$ for the superconducting samples, measured in a field of $\mu_0 H = 2$ mT. Evidence of bulk superconductivity was observed for $0.06 \le x \le 0.12$. The superconducting volume fraction reaches over 30% for $x = 0.1$ and $x = 0.12$. Furthermore, a kink can be tracked around $T_{\mathrm{N}}^{\mathrm{Ce}} \approx 4$ K at various doping concentrations (see the arrows for $x = 0.1$ and 0.12). Likely, this corresponds to the AFM transition of Ce in the superconducting state. It is noted that such a magnetic transition of Ce is clearly demonstrated in the specific heat (see below). The superconducting transition temperatures T_{sc}, derived from the electrical resistivity and magnetic susceptibility, are summarized in Table I.

Magnetic susceptibility of the non-superconducting samples, measured in a magnetic field of $\mu_0 H = 0.1$ T, is presented in Fig.4. Over a wide doping range of $0 \le x \le 0.8$, the magnetic susceptibility $\chi(T)$ consistently shows a pronounced peak around $T_{\mathrm{N}}^{\mathrm{Ce}} \approx 4$ K, which is attributed to the AFM transition of Ce. For $x \ge 0.75$, the magnetic susceptibility $\chi(T)$ shows a sharp increase at a temperature $T_{\mathrm{C}}^{\mathrm{Co}}$ that increases with x, reaching 75 K at $x = 1$. Moreover, the zero-field cooling (ZFC) and field cooling (FC) data become separated below $T_{\mathrm{C}}^{\mathrm{Co}}$ (see, for example, the curves of $x = 0.75$ in Fig.4(a) and $x = 1$ in Fig.5). All these indicate that the Co-ions undergo a FM transition at $T_{\mathrm{C}}^{\mathrm{Co}}$, which value can be obtained from the derivatives of $\mathrm{d}\chi/\mathrm{d}T$ as shown in the inset of Fig.4(b). In this doping region, the magnetic transition associated with Ce $4f$-electrons becomes

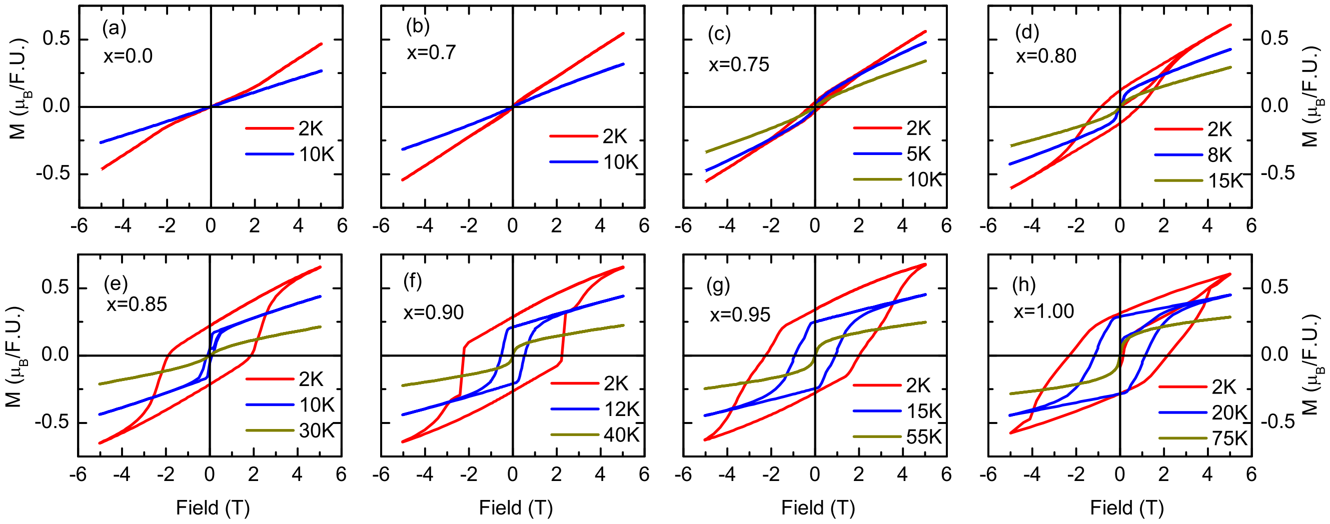

FIG. 6. (Color online) Field dependence of the magnetization $M(H)$ at various temperatures for $\mathrm{CeFe}_{1-x}\mathrm{Co}_x\mathrm{AsO}$, $0 \leq x \leq 1$. The dark yellow curves are measured around the Curie temperature $T_{\mathrm{C}}^{\mathrm{Co}}$.

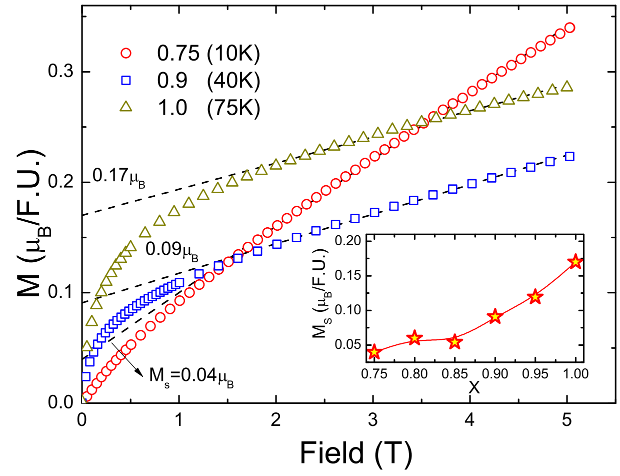

FIG. 7. (Color online) $M(H)$ curves around the Curie temperature $T_{\mathrm{C}}^{\mathrm{Co}}$ for $\mathrm{CeFe}_{1-x}\mathrm{Co}_x\mathrm{AsO}$, $x = 0.75, 0.9$ and 1. The dashed lines describe the methods of deriving the saturated moments. The inset plots the saturated moments as a function of Co concentration.

indiscernible but one can still determine it after properly subtracting a FM background of Co (see below for details). In the high temperature range, the magnetic susceptibility $\chi(T)$ can be well described by the Curie-Weiss law: $\chi(T) = \chi_0 + C/(T - \theta_p)$, with χ_0 being a temperature-independent susceptibility, C the Curie constant and θ_p the paramagnetic Curie temperature. In the inset of Fig.4(a), we plot $1/\chi(T)$ versus T for $x = 0.75$ and 1, respectively. Here the red lines show the fits to Curie-Weiss law. For $x = 0.75$, the effective moment and paramagnetic Curie temperature are derived to be 2.54 μ_B and -31.2 K, respectively; the former one is very close to the free-ion moment of Ce. On the other hand, the effective moment reaches 2.81 μ_B for $x = 1$, which is significantly larger than that of the free-ion moment of Ce. According to $\mu_{\mathrm{eff}} = (\mu_{\mathrm{Co}}^2 + \mu_{\mathrm{Ce}}^2)^{1/2}$, we can estimate the effective moment of Co, which gives μ_{Co}=1.2 μ_B, being consistent with that reported in Ref.14.

As mentioned above, the magnetic transition of Ce is concealed by the strong FM background of Co for $x \geq 0.85$. In order to track the magnetic transition of Ce in these samples, we need subtract the FM contributions of Co-ions which can be approximated by applying an appropriate polynomial fit to the experimental data in a temperature region below $T_{\mathrm{C}}^{\mathrm{Co}}$. As an example, we show the magnetic susceptibility $\chi(T)$ (both ZFC and FC) of CeCoAsO in Fig.5. The hump in the ZFC data is likely caused by the FM domain effect. The solid lines represents a polynomial fit to the experimental data between 20 K and 50 K, which can be approximately treated as the FM contributions of Co. The so-subtracted magnetic susceptibility $\Delta\chi$ of Ce-ions is plotted in the inset of Fig.5, which allow us to determine the magnetic transition of Ce from the maximum of $\Delta\chi(T)$ as marked by the arrow in the inset. Here the magnetic transition is again broadened attributed to the possible polarization effect of Co-moments. Nevertheless, the peak structure of $\Delta\chi(T)$ still indicates an AFM-type transition of Ce-moments at $T_{\mathrm{N}}^{\mathrm{Ce}}$.

Figure 6 presents the field dependence of the magnetization $M(H)$ at various temperatures. For $x \leq 0.7$, $M(H)$ exhibits linear behavior without hysteresis, suggesting the absence of spontaneous magnetization. In CeFeAsO (Fig.6a), a kink was observed around 2 T at $T = 2$ K which might correspond to a spin-flop transition of Ce.[6] While the Co-ions become ferromagnetically

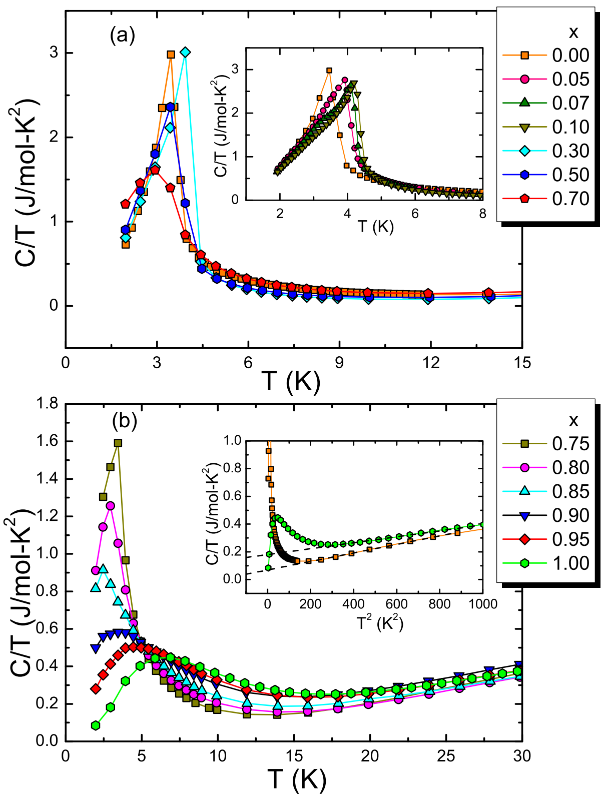

FIG. 8. (Color online) Temperature dependence of the specific heat $C(T)/T$ at zero field for $\mathrm{CeFe}_{1-x}\mathrm{Co}_x\mathrm{AsO}$, $0 \leq x \leq 1$. Inset of (a) shows the data for low Co concentrations ($0 \leq x \leq 0.1$). Inset of (b) plots $C(T)/T$ versus T^2 for CeFeAsO and CeCoAsO. The dashed lines are fits to $C/T = \gamma_0 + \beta T^2$.

ordered at $x \geq 0.75$, the magnetization $M(H)$ shows an obvious hysteresis loop at temperatures below $T_{\mathrm{C}}^{\mathrm{Co}}$; its size increases with either increasing Co concentration or decreasing temperature. From Fig.7, one can see that the saturated moments, derived by extrapolating the linear part of the $M(H)$ curves at temperatures near $T_{\mathrm{C}}^{\mathrm{Co}}$ to zero field, increase with increasing Co concentration, reaching $0.17\mu_B$ at $x = 1$ (see the inset). Similar results were also reported in LaCoAsO, NdCoAsO and SmCoAsO compounds with a saturated moment of $0.46\mu_B$, $0.20\mu_B$ and $0.18\mu_B$ respectively.[21–23] The saturated moment of Co in these compounds is much smaller than $3\mu_B/\mathrm{Co}^{2+}$ as expected for the localized high spin state of Co^{2+}, meaning that the ferromagnetism of Co is itinerant in nature. It is noted that such a large hysteresis was not observed in other *Re*CoAsO compounds except for CeCoAsO.[21–24]

D. Heat Capacity

In order to further characterize the magnetic order of Ce $4f$-electrons in $\mathrm{CeFe}_{1-x}\mathrm{Co}_x\mathrm{AsO}$, we also measured the temperature dependence of specific heat $C(T)$. Figure 8 presents the low-temperature specific heat $C(T)/T$ of several representative doping concentrations. One can see that the specific heat $C(T)/T$ shows a λ-type transition for $x \leq 0.8$, characteristic of a typical AFM transition. The transition temperatures are consistent with those derived from the electrical resistivity and magnetic susceptibility as shown above. In previous measurements of neutron scattering and muon spin relaxation, it was found that there exists a strong coupling between Ce-$4f$ and Fe-$3d$ electrons in CeFeAsO.[25,26] In this case, suppression of the SDW transition of Fe may have a significant impact on the magnetic order of Ce. To confirm it, we have performed a detailed measurement of low temperature specific heat for $x \leq 0.1$. As seen in the inset of Fig.8(a), the AFM transition of Ce indeed shifts to higher temperature while suppressing the SDW transition of Fe by Fe/Co substitution, indicating a kind of competing interaction between Ce $4f$- and Fe $3d$-electrons. It is noted that, in the electrical resistivity $\rho(T)$, the SDW transition is hardly visible for $x > 0.06$. However, the continuous increase of $T_{\mathrm{N}}^{\mathrm{Ce}}$ up to $x = 0.1$ may indicate that the critical doping concentration for suppressing the SDW transition is around $x \simeq 0.1$, which is compatible if we extrapolate the SDW-phase boundary in the phase diagram as shown in Fig.9. Furthermore, the specific heat $C(T)/T$ of the superconducting samples shows a pronounced magnetic transition of Ce around $T_{\mathrm{N}}^{\mathrm{Ce}} \approx 4$ K.

With further increasing Co content, the AFM transition of Ce hardly depends on the doping concentration up to $x = 0.8$. Above that, the transition is significantly broadened and its maximum is slightly shifted towards higher temperatures with increasing x, being similar to the resistive results. Such behavior is likely attributed to the Co-induced polarization on Ce-moments, which may take place prior to the AFM order of Ce at $T_{\mathrm{N}}^{\mathrm{Ce}}$. The specific heat data can be fitted by $C/T = \gamma_0 + \beta T^2$ at temperatures above the magnetic transition of Ce (see the dashed lines in the inset of Fig.8(b)), from which one can estimate the Sommerfeld coefficient γ_0. The derived γ_0 values are summarized in the inset of Fig.9, which is nearly a constant for $0 \leq x \leq 0.7$, but then increases with further increasing x. In comparison with CeFeAsO ($\gamma_0 = 36$ mJ/mol K^2),[27] the γ_0 value of CeCoAsO is largely enhanced ($\gamma_0 \simeq 186$ mJ/mol-K^2), implying an increase of the hybridization between $4f$- and $3d$-electrons upon substituting Fe with Co.

E. Phase Diagram and Discussion

Based on the above experimental data, in Fig.9 we present a magnetic and superconducting phase diagram for $\mathrm{CeFe}_{1-x}\mathrm{Co}_x\mathrm{AsO}$ ($0 \leq x \leq 1$). CeFeAsO is a bad metal, in which Fe $3d$- and Ce $4f$-electrons are antiferromagnetically ordered below 150 K and 4 K, respectively. Upon substituting Fe with Co, the magnetic order of Fe $3d$-electrons is suppressed around $x \approx 0.1$ (marked

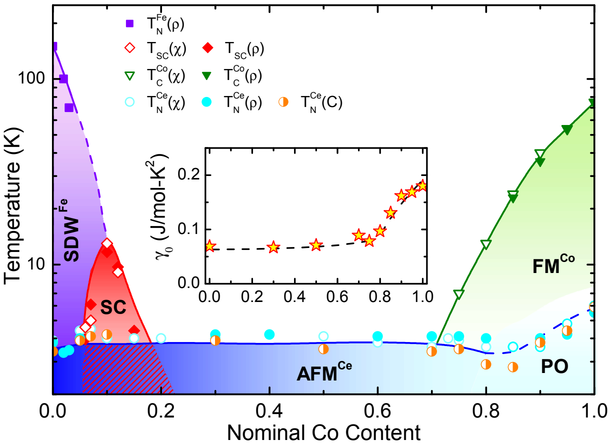

FIG. 9. (Color online) The magnetic and superconducting phase diagram of $CeFe_{1-x}Co_xAsO$, plotted as a function of nominal Co content. Various symbols denote different types of transition temperatures. The lines are guides to the eyes. The inset plots the Sommerfeld coefficient γ_0 as a function of Co concentration.

by SDW^{Fe}) and superconductivity appears in a narrow range of $0.05 < x < 0.20$ (marked by SC), indicating that the formation of superconductivity is closely related to the magnetism of Fe in these compounds. At lower temperatures, Ce $4f$-electrons undergo an AFM transition in the entire doping-range (marked by AFM^{Ce}); the Néel temperature T_N^{Ce} slightly increases with suppressing the SDW transition of Fe and then remains nearly unchanged up to $x = 0.8$. With further increasing Co-content ($x \geq 0.75$), the Co $3d$-electrons form a long range FM order which Curie temperature eventually increases with x, reaching $T_C^{Co} \simeq 75$ K in CeCoAsO (marked by FM^{Co}). On the Co-rich side, the Co-ferromagnetism has a strong polarization effect on the AFM order of Ce (marked by PO).

As shown above, the 1111-type iron pnictides exhibit rich magnetic and superconducting properties via elemental substitutions. Different from $CeFe_{1-x}Co_xAsO$, superconductivity was only observed around $x = 0.3$ in $CeFeAs_{1-x}P_xO$, which seems to coexist with ferromagnetism of Ce below 4 K.[8] The magnetic order of Ce persists up to $x = 0.9$ in $CeFeAs_{1-x}P_xO$, but it changes from an AFM- to a FM-type order while the SDW transition of Fe is suppressed around $x \simeq 0.3$.[6–8] On the other hand, the AFM order of Ce-ions is remarkably robust against Fe/Co substitution. Its ordering temperature T_N^{Ce} increases with x while suppressing the SDW transition of Fe, followed by a nearly unchanged value. The persistence of the Ce-moment AFM order with a slight variation in T_N^{Ce} on the Co-doping seems to contradict the Kondo physics, which effect would be enhanced when the interlayer distance is compressed by the Fe/Co substitution as evidenced from the enhancement of the Sommerfeld coefficient in CeCoAsO ($\gamma_0 \sim 200$ mJ/mol-K^2).[14] This is possibly due to the polarization of Co-atoms caused by the spin-orbit coupling which competes with the Kondo effect. The resulting AFM exchange interaction between Co $3d$- and Ce $4f$-electrons is thus anisotropic in the spin space. The multi-orbital characteristics may also add complications to the interplay among various intralayer and interlayer exchange interactions, leading to diverse behavior in the $3d$-$4f$ electron pnictides. For example, in other ReCoPnO systems, e.g., Re = Sm and Nd,[22,24,28] the interlayer d-f exchange interaction is strong enough to realign the Co moments, leading to a subsequent AFM transition of Co at a lower temperature. Such transitions and magnetic structures have recently been proposed from the neutron scattering in NdCoAsO.[12,22] However, in $CeFe_{1-x}Co_xAsO$, Ce-ions carry a small magnetic moment and it shows a relatively weak lattice shrinkage along the c-axis while substituting Fe with Co; the resulting AFM exchange interaction is likely not sufficiently strong to realign the Co moments. Instead, the Ce moments are partially polarized by the internal field of Co. Further investigations based on model calculations and elastic neutron scattering on the Co-rich side is highly desirable in order to clarify the magnetic structures of $3d$- and $4f$-electrons in this system.

IV. CONCLUSION

In summary, we have systematically studied the transport, magnetic and thermodynamic properties on a series of $CeFe_{1-x}Co_xAsO$ ($0 \leq x \leq 1$) polycrystalline samples and presented a complete doping-temperature phase diagram. It is found that the SDW transition associated with Fe $3d$-electrons is quickly suppressed upon substituting Fe with Co and superconductivity shows up in a narrow doping range ($0.05 < x < 0.2$). At lower temperatures, Ce $4f$-electrons undergo an AFM-type magnetic transition, which Néel temperature is slightly increased while suppressing the SDW-transition of Fe, but then becomes nearly unchanged with further increasing Co-content. For $x \geq 0.75$, Co electrons form a long-range FM order, which transition temperature increases with increasing x and reaches $T_C^{Co} \approx 75$ K in CeCoAsO. Evidence of a strong polarization effect of the Co-ferromagnetism on Ce atoms is observed on the Co-rich side. Our findings suggest that the delicate interplay of $3d$-$4f$ electrons arising from the competition of electron hybridizations and magnetic exchange coupling leads to remarkably rich physics in the iron-based compounds.

ACKNOWLEDGMENTS

We would like to thank M. Salamon, C. Geibel, E. D. Bauer, R. E. Baumbach, F. Ronning, F. C. Zhang, G. H. Cao and Z. A. Xu for useful discussions. This work is supported by National Basic Research Program of

China (Nos: 2009CB929104, 2011CBA00103), National Science Foundation of China (Nos: 10934005, 11174245, 11274084), Zhejiang Provincial Natural Science Foundation of China (Z6110033), and the Fundamental Research Funds for the Central Universities of China.

---

[*] hqyuan@zju.edu.cn

[1] Y. Kamihara, T. Watanabe, M. Hirano, and H. Hosono, J. Am. Chem. Soc. **130**, 3296 (2008).

[2] See reviews, e.g., H. H. Wen, Adv. Mater. **20**, 3764 (2008); M. V. Sadovskii, Physics-Uspekhi **51**, 1201; J. Paglione and R. L. Greene, Nature physics **6**, 645 (2010).

[3] G. F. Chen, Z. Li, D. Wu, G. Li, W. Z. Hu, J. Dong, P. Zheng, J. L. Luo, and N. L. Wang, Phys. Rev. Lett. **100**, 247002 (2008).

[4] J. Zhao, Q. Huang, C. de La Cruz, S. Li, J. W. Lynn, Y. Chen, M. A. Green, G. F. Chen, G. Li, Z. Li, J. L. Luo, N. L. Wang, and P. C. Dai, Nature Materials **7**, 953 (2008).

[5] E. M. Brüning, C. Krellner, M. Baenitz, A. Jesche, F. Steglich, and C. Geibel, Phys. Rev. Lett. **101**, 117206 (2008).

[6] Y. K. Luo, Y. K. Li, S. Jiang, J. H. Dai, G. H. Cao, and Z. A. Xu, Phy. Rev. B **81**, 134422 (2010).

[7] C. de La Cruz, W. Z. Hu, S. Li, Q. Huang, J. W. Lynn, M. A. Green, G. F. Chen, N. L. Wang, H. A. Mook, Q. M. Si, and P. C. Dai, Phys. Rev. Lett. **104**, 017204 (2010).

[8] A. Jesche, T. Förster, J. Spehling, M. Nicklas, M. de Souza, R. Gumeniuk, H. Luetkens, T. Goltz, C. Krellner, M. Lang, J. Sichelschmidt, H. H. Klauss, and C. Geibel, Phys. Rev. B **86**, 020501 (2012).

[9] L. D. Zhao, D. Berardan, C. Byl, L. P. Gaudart, and N. Dragoe, J. Phys.: Condens. Matter **22**, 115701 (2010).

[10] A. S. Sefat, A. Huq, M. A. McGuire, R. Jin, B. C. Sales, D. Mandrus, L. M. D. Cranswick, P. W. Stephens, and K. H. Stone, Phys. Rev. B **78**, 104505 (2008).

[11] P. M. Shirage, K. Miyazawa, H. Kito, E. H. Isaki, and A. Iyo, Physica C: Superconductivity **469**, 898 (2009).

[12] A. Marcinkova, D. A. M. Grist, I. Margiolaki, T. C. Hansen, S. Margadonna, and J. W. G. Bos, Phys. Rev. B **81**, 064511 (2010).

[13] C. Wang, Y. K. Li, Z. W. Zhu, S. Jiang, X. Lin, Y. K. Luo, S. Chi, L. J. Li, Z. Ren, M. He, H. Chen, Y. T. Wang, Q. Tao, G. H. Cao, and Z. A. Xu, Phys. Rev. B **79**, 054521 (2009).

[14] R. Sarkar, A. Jesche, C. Krellner, M. Baenitz, C. Geibel, C. Mazumdar, and A. Poddar, Phys. Rev. B **82**, 054423 (2010).

[15] C. Krellner, U. Burkhardt, and C. Geibel, Physica B: Condensed Matter **404**, 3206 (2009).

[16] T. Shang, L. Yang, N. Cornell, F. Ronning, A. Howard, Y. Chen, L. Jiao, J. Chen, J. D. Thompson, A. Zakhidov, M. B. Salamon and H. Q. Yuan, submitted.

[17] J. Dong, H. J. Zhang, G. Xu, Z. Li, G. Li, W. Z. Hu, D. Wu, G. F. Chen, X. Dai, J. L. Luo, Z. Fang and N. L. Wang, Europhys. Lett. **83**, 27006 (2008).

[18] T. Shang, L. Jiao, J. H. Dai, H. Q. Yuan, F. F. Balakirev, W. Z. Hu and L. N. Wang, arxiv: 1209.4529.

[19] S. Araki, M. Nakashima, R. Settai, T. C. Kobayashi and Y. Onuki, J. Phys.: Condens. Matter **14**, L377 (2002).

[20] Z. Hossain, H. Ohmoto, K. Umeo, F. Iga, T. Suzuki, T. Takabatake, N. Takamoto and K. Kindo, Phys. Rev. B **60**, 10383 (1999).

[21] H. Yanagi, R. Kawamura, T. Kamiya, Y. Kamihara, M. Hirano, T. Nakamura, H. Osawa, and H. Hosono, Phys. Rev. B **77**, 224431 (2008).

[22] M. A. McGuire, D. J. Gout, V. O. Garlea, A. S. Sefat, B. C. Sales, and D. Mandrus, Phys. Rev. B **81**, 104405 (2010).

[23] V. P. S. Awana, I. Nowik, A. Pal, K. Yamaura, E. T. Muromachi, and I. Felner, Phys. Rev. B **81**, 212501 (2010).

[24] H. Ohta, and K. Yoshimura, Phys. Rev. B **80**, 184409 (2009).

[25] S. Chi, D. T. Adroja, T. Guidi, R. Bewley, S. Li, J. Zhao, J. W. Lynn, C. M. Brown, Y. Qiu, G. F. Chen, J. L. Lou, N. L. Wang, and P. C. Dai, Phys. Rev. Lett. **101**, 217002 (2008).

[26] H. Maeter, H. Luetkens, Y. G. Pashkevich, A. Kwadrin, R. Khasanov, A. Amato, A. A. Gusev, K. V. Lamonova, D. A. Chervinskii, R. Klingeler, C. Hess, G. Behr, B. Büchner, and H. H. Klauss, Phys. Rev. B **80**, 094524 (2009).

[27] S. Riggs, C. Tarantini, J. Jaroszynski, A. Gurevich, A. Palenzona, M. Putti, T. D. Nguyen, and M. Affronte, Phys. Rev. B **80**, 214404 (2009).

[28] Anand Pal, S. S. Mehdi, M. Hussain, B. Gahtori and V. P. S. Awana, J. Appl. Phys. **110**, 103913 (2011).